Seismic-Resilient Electric Power Distribution Systems: Harnessing the Mobility of Power Sources

Zijiang Yang, *Student Member, IEEE*, Payman Dehghanian, *Member, IEEE*, and Mostafa Nazemi, *Student Member, IEEE*

***Abstract*—Mobile power sources (MPSs), including mobile emergency generators, truck-mounted mobile energy storage systems, and electric vehicles, have great potentials to be employed as grid-support resources during power grid emergency operating conditions to supply the critical loads and enhance the resilience of distribution system (DS) via a swift disaster restoration. We here investigate the MPS dispatch (i.e., routing and scheduling) in coordination with DS dynamic network reconfiguration. We propose a two-stage restoration scheme to facilitate the DS restoration following the high-impact low-probability (HILP) seismic disasters. In the first stage, a seismic hazard is simulated through a Monte Carlo simulation engine to estimate the unavailability of power distribution branches under a suite of seismic force scenarios. In the second stage, a mixed-integer nonlinear programming (MINLP) optimization model is formulated for DS restoration that cooptimizes the routing and scheduling of MPSs and DS dynamic network reconfiguration. The MINLP model is then linearized to a mixed-integer linear programming model to reduce the computation complexity, where the seismic-resilience recovery strategies are generated at different timescales. The efficacy of the proposed method is evaluated on the IEEE 33-node test system and the results verify a significant reduction in the load outages and an improved power system resilience to HILP earthquakes.**

***Index Terms*—Distribution systems (DS), dynamic reconfiguration, high-impact low-probability (HILP) hazards, mobile power sources (MPSs), routing and scheduling, seismic resilience.**

NOMENCLATURE

A. Sets and Indices

$i, j \in \mathbf{B}$	Indices/set of nodes.
$m \in \mathbf{M}$	Indices/set of mobile power sources (MPSs).
$t, \tau \in \mathbf{T}$	Indices/set of time periods.
$(i, j) \in \mathbf{L}$	Indices/set of branches.
$N_{\mathbf{B}}, N_{\mathbf{T}}, N_{\mathbf{L}}$	Number of all nodes, time periods, and branches.
$\mathbf{B}^{\text{sub}}$	Set of substation nodes.
$\mathbf{B}_m$	Set of candidate nodes that can be connected to MPS m.
$\mathbf{B}_t^{\text{source}}$	Set of nodes that are selected to be the sources of the fictitious flows at time t.
$\mathbf{L}^{\text{switch}}$	Set of branches equipped with remotely controlled switches.
$\mathbf{L}_t^{\text{damaged}}$	Set of branches that are damaged and have not been repaired at time t.
$\mathbf{G} \in \mathbf{M}$	Set of all mobile emergency generators (MEGs).
$\mathbf{S} \in \mathbf{M}$	Set of all mobile energy storage systems (MESSs).
$\mathbf{V} \in \mathbf{M}$	Set of all mobile electric vehicle (EV) fleets.
$\mathbf{M_i}$	Set of MPSs that can be connected to node i.

B. Parameters and Constants

χ_i	Priority of the load demanded at node i.
$\beta_{ij,t}$	Binary damage status of the branch (i, j) at time t (1 if the branch is undamaged or has been repaired, 0 otherwise).
$P_{i,t}^{\text{demand}}$	Real power demand of node i at time t (kW).
$Q_{i,t}^{\text{demand}}$	Reactive power demand of node i at time t (kVar).
α_{ij}^0	Binary parameter representing the initial status of branch (i, j) (1 if the branch is connected, 0 otherwise).
N_t^{island}	Number of islands due to the damaged and unrepaired branches at time t.
N_i^{mps}	Number of MPSs that are allowed to be connected to node i.
$T_{m,ij}^{\text{travel}}$	Travel time of MPS m from node i to node j.
Δt	Duration of one time period.
M	Large enough positive number.
$\underline{\text{SOC}}_m$	Minimum state of charge (SOC) of MESS or EV fleet m (kWh).
$\overline{\text{SOC}}_m$	Maximum SOC of the MESS or EV fleet m (kWh).
$\overline{P}_m^{\text{ch}}, \overline{P}_m^{\text{dch}}$	Maximum charging and discharging power of MESS or EV fleet m (kW, kVar).
$\overline{P}_m, \overline{Q}_m$	Maximum real and reactive power output of MPS m (kW, kVar).
$\overline{P}_{ij}, \overline{Q}_{ij}$	Real and reactive power capacity of branch (i, j) (kW, kVar).

Manuscript received July 8, 2019; revised November 17, 2019; accepted February 2, 2020. Date of publication February 10, 2020; date of current version April 24, 2020. Paper 2019-PSEC-0717.R1, presented at the 2019 IEEE Industry Applications Society Annual Meeting, Baltimore, MD USA, Sep. 29–Oct. 3, and approved for publication in the IEEE TRANSACTIONS ON INDUSTRY APPLICATIONS by the Power Systems Engineering Committee of the IEEE Industry Applications Society. *(Corresponding author: Payman Dehghanian.)*

Zijiang Yang is with the China Energy Engineering Group, Guangdong Electric Power Design Institute Company, Ltd., Guangdong 510663, China (e-mail: yangzijiang5927@163.com).

Payman Dehghanian and Mostafa Nazemi are with the Department of Electrical and Computer Engineering, George Washington University, Washington, DC 20052 USA (e-mail: payman@gwu.edu; mostafa_nazemi@gwu.edu).

Color versions of one or more of the figures in this article are available online at http://ieeexplore.ieee.org.

Digital Object Identifier 10.1109/TIA.2020.2972854

r_{ij}, x_{ij} Resistance and reactance of branch (i, j) (Ω).
$\underline{V\text{sqr}}_i$ Minimum squared voltage magnitude at node i (kV^2).
$\overline{\text{Vsqr}}_i$ Maximum squared voltage magnitude at node i (kV^2).
C_m^{tr} Transportation cost coefficient of MPS m.
C_m^{P} Power rating price of MESS or EV fleet m (\$/kWh).
k_m Degradation slope of MESS or EV feelt m.
δ_m Generation cost coefficient of MEG m.
$\eta_m^{\text{ch}}, \eta_m^{\text{dch}}$ Charging and discharging efficiency of MESS or EV fleet m.
P_m^{travel} Energy Consumption rate of EV fleet m when traveling (kW).
$d_{i,t}^{\text{fic}}$ Fictitious load of node i at time t.

C. Functions and Variables

$pd_{i,t}, qd_{i,t}$ Real and reactive power demand supplied at node i at time t (kW, kVar).
$pg_{i,t}, qg_{i,t}$ Real and reactive power at substation node i at time t (kW, kVar).
$pf_{ij,t}, qf_{ij,t}$ Real and reactive power flow on branch (i, j) at time t (kW, kVar).
$\text{SOC}_{m,t}$ SOC of MESS or EV fleet m at time t (kWh).
$p_{m,t}^{\text{ch}}, p_{m,t}^{\text{dch}}$ Charging and discharging power of MESS or EV fleet m at time t (kW).
$p_{m,t}, q_{m,t}$ Real and reactive power output of MPS m at time t (kW, kVar).
$p_{i,t}^{\text{mps}}, q_{i,t}^{\text{mps}}$ Real and reactive power output of MPS at node i (kW, kVar).
$V\text{sqr}_{i,t}$ Squared voltage magnitude at node i at time t (kV^2).
$fl_{ij,t}$ Fictitious flow on branch (i, j) at time t.
$fg_{i,t}$ Fictitious supply at source node i at time t.

D. Binary Variables

$\alpha_{ij,t}$ Connection status of branch (i, j) at time t (1 if the branch is connected, 0 otherwise).
$c_{m,t}, d_{m,t}$ Charging and discharging status of MESS or EV fleet m at time t (1 if it is charging or discharging, 0 otherwise).
$\varphi_{m,t}$ Traveling status of MPS m at time t (1 if the MPS is traveling, 0 otherwise).
$\mu_{m,i,t}$ Connection status of MPS m to node i at time t (1 if connected, 0 otherwise).

I. Introduction

In THE recent years, more frequent realization of the high-impact low-probability (HILP) natural disasters, such as hurricanes, windstorms, earthquakes, etc., have resulted in prolonged electricity outages, excessive equipment damages, and even more severe economic loss and disruptions in our modern society [1]–[4]. Earthquakes are the most unpredictable hazards that can cause striking damages in radial power distribution systems (DS). Among the past records on disastrous earthquakes, one can highlight the Loma Prieta earthquake in the greater San Francisco Bay Area in California in 1989 that caused \$6 billion in property damage [5], the Northridge earthquake that struck Los Angeles on January 17, 1994, affecting 2.5 million local customers [6], Hanshin-Awaji region that was struck by the Hyogo-ken Nanbu earthquake on January 17, 1995, resulting approximately in 2.6 million households out of power services [7], the severe Bam earthquake in 2003 causing \$90 million electricity reconstruction in Iran [8], the Wenchuan earthquake in 2008 that caused extreme damages in 966 substations, 274 transmission lines at multiple voltage levels and 1700 circuits damages [9], the Tohoku earthquake in 2011 impacting 8.9 million households in 18 prefectures among 4 electric power companies [10], and recently in 2017 in Iran, the Sarpol-e Zahab earthquake with 7.3 moment magnitude resulting in a prolonged city-wide blackout for weeks [11].

As occurrence of such catastrophic HILP-caused electricity outages has been observed to be on the rise over the past decade [12], [13], it calls for developing effective mechanisms that ensure a continuous and resilient supply of electricity to the end customers when dealing with the aftermath of seismic hazards [14]. Power DS resilience to HILP events can be elevated by holistic planning, operation, and control of microgrids in which critical loads can be supplied during emergencies [15], [16]. Microgrids, as the physical islands (PI) in a local area, can be formed by utilizing distributed energy resources (DERs) to provide continuous power supply to electric utilities and customers [17]. Microgrids as an efficient mechanism to supply the critical loads during emergencies are studied in [18] where the restoration problem is transformed to a maximum coverage problem considering DERs' dynamic performance. The DERs, however, are typically deployed at fixed locations across the grid and, thus, are only able to support the local load points within a PI and maybe some in neighboring PIs, but certainly not the demanded loads in further away PIs. Comparing with stationary microgrids with fixed-location DERs, mobile power sources (MPSs), which include mobile emergency generators (MEGs), electric vehicles (EVs), and truck-mounted mobile energy storage systems (MESSs), offer greater advantages as the grid-support resources to boost the DS resilience primarily driven by their mobility. The application of MPSs for enhanced resilience of DS has been studied in several research efforts [19]–[21]. Routing and scheduling of EVs is studied in [22] where EVs can be charged to store energy not only to meet its own transportation requirements, but also as an emergency power source to supply electricity to critical loads during emergencies [22]. Scheduling the charging and discharging of EVs is studied in [23] aiming to enhance the DS resilience against natural disasters. In [24], vehicle-to-home technology, as a simplified variation of the vehicle-to-grid mechanism, is proposed as a backup power source to support the end customers during grid interruptions. MEG is studied in [17] and [25] to recover the weather-caused outages and improve power system resilience. Following an HILP hazard, the configuration of the DS may change due to the unavailability of some distribution branches and other elements. DS network reconfiguration plays a significant role in rerouting and delivering the power from MPSs to critical loads by switching some branches ON and OFF. The distribution branches can be equipped with remotely

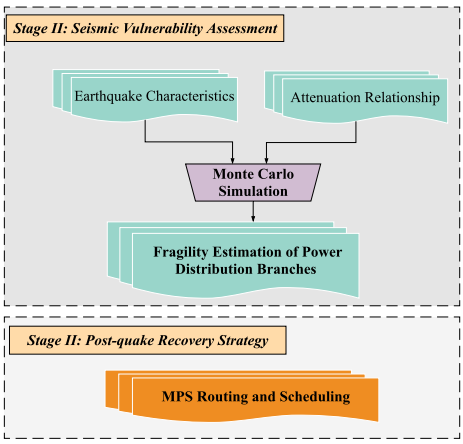

Fig. 1. Architecture of the proposed framework for earthquake resilience.

controlled switches (RCS) that facilitate a network reconfiguration as emergency operating conditions unfold. Several models of DS network reconfiguration have been studies in the literature to improve the grid resilience in the face of emergencies [26]–[29].

In this article, a suite of HILP seismic hazards is generated by Monte Carlo simulation (MCS) engine, which generates a huge set of earthquake scenarios to estimate the vulnerability of power distribution branches in the face of severe seismic forces. Then, a mixed-integer nonlinear programming (MINLP) model is proposed for routing and scheduling of MPSs coordinated with the DS network reconfiguration to improve the DS resilience against seismic hazards. The MINLP model is further linearized into a mixed-integer linear programming (MILP) model to decrease the computation complexity. Multiple types of MPSs, e.g., MEGs, MESSs, and EVs, are dispatched considering the repair schedules of the damaged branches to facilitate the DS restoration process.

The rest of this article is organized as follows. A big picture of the proposed model for MPSs dynamic dispatch and DS reconfiguration is presented in Section II. The proposed MILP formulation is presented in Section III. Numerical results are extensively analyzed and reported in Section IV, followed by discussion on practical implications of the proposed methodology in Section V. Finally, Section VI concludes this article.

II. Big Picture: Proposed Architecture for DS Resilience to Seismic Hazards

A. Seismic Hazard Characterization and Overhead Lines' Vulnerability Assessment

The proposed architecture for power grid resilience against HILP earthquakes is demonstrated in Fig. 1. According to Fig. 1, the first step toward simulation of HILP seismic hazards is to generate a significant number of scenarios by MCS to estimate the peak ground acceleration (PGA) as a seismic intensity parameter at the location of power distribution branches. Fault mechanism, source specification, distance from the seismic source, the direction of seismic waves propagation, the properties of soil and sediments, and the geology and topology effects of the studied case are among factors that should be considered within an analytical attenuation relationship (AR) to properly model the attenuation of seismic waves energy. According to Nuttli [30], a general formulation of the AR can be defined as follows:

$$\ln(\xi) = f(M) + f(R) + f(Z) + \epsilon \tag{1}$$

where ξ is the ground motion parameter, M is the earthquake magnitude, R is the distance between the source of earthquake and the studied case, and ϵ is a random error with mean value of zero and standard deviation of σ representing the uncertainty in ξ. Other parameters, such as the site conditions, fault mechanism, sediment thickness, etc., can be mathematically modeled in a general form as $f(Z)$. Since power distribution branches do not have the same response to earthquake shocks, five damage states—*none*, *slight*, *moderate*, *extensive*, and *complete damage*—are introduced in this article to assess the fragility of power distribution branches in the face of earthquakes [31]. According to the work in [32], application of fragility curves is pursued in this article by which the unavailability of power distribution line sections can be assessed. Each fragility curve is characterized by a median and log-normal standard deviation (σ) of the PGA parameter, which corresponds to the damage state thresholds and associated variability. The probability of residing in or exceeding a state of structural damage (γ) is described as follows:

$$P\left[\gamma|S_d\right] = \Phi\left[\frac{1}{\sigma_\gamma}\ln\left(\frac{S_d}{\overline{S}_{d,\gamma}}\right)\right] \tag{2}$$

where S_d is the spectral displacement, $\overline{S}_{d,\gamma}$ is its median value, σ_γ is the standard deviation corresponding to the natural logarithm of the spectral displacement at which a structure reaches the damage state threshold, and Φ is the standard cumulative normal distribution function.

B. Routing and Scheduling of MPS for Enhanced Resilience

Based on Fig. 2, the unavailability of some distribution branches following a seismic HILP event results in a number of PIs in which some or all load points are disconnected from the main grid. The optimal scheduling and routing of MPS can be achieved via the proposed optimization formulation with the aim of enhancing the DS resilience. Having identified the damaged branches in Stage I, the MPS can be moved to other PIs in which some portions of critical loads can be recovered by the excessive power provided by MPS. Meanwhile, the other damaged branches are repaired by repair crews and this loop is repeated until all damaged branches are repaired and all load points are supplied in the main grid. The system is then fully restored and the DS resilience function reaches its maximum.

III. Problem Formulation

This section presents an extensive formulation for routing and scheduling of MPS. Motivated by Lei *et al.* [23], the objective

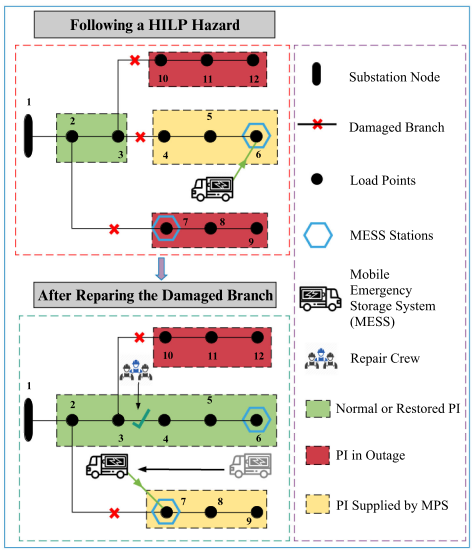

Fig. 2. Optimal routing and scheduling of MPSs following a seismic hazard.

function (3) includes four terms, which are as follows:

$$\max\left(\sum_{t\in\mathbf{T}}\sum_{i\in\mathbf{B}}\chi_i\cdot pd_{i,t}-\sum_{t\in\mathbf{T}}\sum_{m\in\mathbf{M}}C_m^{\mathrm{tr}}\cdot\varphi_{m,t}-\sum_{t\in\mathbf{T}}\sum_{m\in\{\mathbf{S},\mathbf{V}\}}\left|\frac{k_m}{100}\right|\cdot C_m^{\mathrm{P}}\cdot\left(p_{m,t}^{\mathrm{ch}}+p_{m,t}^{\mathrm{dch}}\right)-\sum_{t\in\mathbf{T}}\sum_{m\in\mathbf{G}}\delta_m\cdot p_{m,t}\right). \tag{3}$$

The first term is the total supplied load considering the priority of the load points over the entire time period, the second term is the transportation cost of MPSs due to the trips they make during the restoration phase; the third term reflects the cost of battery degradation when charging and discharging; and the last term is the relative cost of the MEG outputs. While there may exist various MPS dispatch strategies, the second term is added to minimize the traveling time of MPSs to avoid unnecessary transportation, the third term is aimed to reduce the battery degradation cost during the restoration phase, and the last term is added to minimize the cost associated with the output power of MEGs. A number of constraints need to be taken into account for the DS restoration problem are as follows.

A. MPS Connection Constraints

Following an HILP disaster, the MPSs rapidly travel and get connected in the PIs to supply electricity where needed. At each time period, MPS can be connected to at most one predetermined candidate node, as enforced in (4). Constraint (5) indicates that the allowed number of MPSs connected to a node is limited to stations' capacity at each candidate node. Constraint (6) states that the MPSs cannot travel to other nodes when connected to a candidate node

$$\sum_{i\in\mathbf{B}_m}\mu_{m,i,t}\le 1\quad\forall m\in\mathbf{M}\quad\forall t\in\mathbf{T} \tag{4}$$

$$\sum_{m\in\mathbf{M}_i}\mu_{m,i,t}\le N_i^{\mathrm{mps}}\quad\forall i\in\bigcup_{m\in\mathbf{M}}\mathbf{B}_m\quad\forall t\in\mathbf{T} \tag{5}$$

$$\varphi_{m,t}=1-\sum_{i\in\mathbf{B}_m}\mu_{m,i,t}\quad\forall m\in\mathbf{M}\quad\forall t\in\mathbf{T}. \tag{6}$$

B. MPS Routing Constraints

Constraint (7) ensures that the MPSs transportation among different DS nodes satisfies the required travel time

$$\mu_{m,i,t+\tau}+\mu_{m,j,t}\le 1\quad\forall m\in\mathbf{M}\quad\forall i,j\in\mathbf{B}_m\quad\forall\tau\le T_{m,ij}^{\mathrm{travel}}\quad\forall t+\tau\le N_{\mathbf{T}}. \tag{7}$$

C. MPS Power Scheduling Constraints

It is assumed that the trunk-mounted MESS and MEG can be refueled with tanker trunk for transportation during the restoration process [33] while EVs consume electric energy when they are in transport. The change in the state of charge (SOC) of MESSs over time is determined by their charging and discharging behaviors, as represented in (8), whereas the SOC of EVs is determined by their charging and discharging as well as travel behaviors (9). Constraint (10) restricts the range of SOC of MESS and EV over all time periods. Constraints (11) and (12), respectively, impose the range of charging and discharging power for MESS and EV according to the corresponding rated power. The charging and discharging powers are both enforced to be zero when MESS and EV are not connected to the DS. Charging and discharging of MESS and EV are mutually exclusive over all time periods, as represented in (13), which indicates that the MPS disconnected from DS can neither charge nor discharge. Constraints (14) and (15) set the range of real and reactive power output of MEG according to its rated power, respectively, and enforce MEG to have zero real and reactive output when it is disconnected from DS

$$\mathrm{SOC}_{m,t}=\mathrm{SOC}_{m,t-1}+\left(\eta_m^{\mathrm{ch}}\cdot p_{m,t}^{\mathrm{ch}}-p_{m,t}^{\mathrm{dch}}/\eta_m^{\mathrm{dch}}\right)\cdot\Delta t\quad\forall m\in\mathbf{S}\quad\forall t\ge 1 \tag{8}$$

$$\mathrm{SOC}_{m,t}=\mathrm{SOC}_{m,t-1}+\left(\eta_m^{\mathrm{ch}}\cdot p_{m,t}^{\mathrm{ch}}-p_{m,t}^{\mathrm{dch}}/\eta_m^{\mathrm{dch}}-\varphi_{m,t}\cdot P_m^{\mathrm{travel}}\right)\cdot\Delta t\quad\forall m\in\mathbf{V}\quad\forall t\ge 1 \tag{9}$$

$$\underline{\mathrm{SOC}}_m\le\mathrm{SOC}_{m,t}\le\overline{\mathrm{SOC}}_m\quad\forall m\in\{\mathbf{S},\mathbf{V}\}\quad\forall t\in\mathbf{T} \tag{10}$$

$$0\le p_{m,t}^{\mathrm{ch}}\le c_{m,t}\cdot\overline{P}_m^{\mathrm{ch}}\quad\forall m\in\{\mathbf{S},\mathbf{V}\}\quad\forall t\in\mathbf{T} \tag{11}$$

$$0\le p_{m,t}^{\mathrm{dch}}\le d_{m,t}\cdot\overline{P}_m^{\mathrm{dch}}\quad\forall m\in\{\mathbf{S},\mathbf{V}\}\quad\forall t\in\mathbf{T} \tag{12}$$

$$c_{m,t}+d_{m,t}\le\sum_{i\in\mathbf{B}_m}\mu_{m,i,t}\quad\forall m\in\{\mathbf{S},\mathbf{V}\}\quad\forall t\in\mathbf{T} \tag{13}$$

$$0\le p_{m,t}\le\sum_{i\in\mathbf{B}_m}\mu_{m,i,t}\cdot\overline{P}_m\quad\forall m\in\mathbf{G}\quad\forall t\in\mathbf{T} \tag{14}$$

$$0\le q_{m,t}\le\sum_{i\in\mathbf{B}_m}\mu_{m,i,t}\cdot\overline{Q}_m\quad\forall m\in\mathbf{G}\quad\forall t\in\mathbf{T}. \tag{15}$$

D. DS Radiality Constraints

Constraints (16)–(19) ensure that the DS remains radial over all time periods. For DS radiality, there are two conditions that need to be satisfied: first, at each PI, the number of connected branches is equal to the total number of nodes in the PI 1, and second, all load points are connected to a determined source node in each PI. The first condition is satisfied in constraint (16). In each PI, one node is considered as a fictitious source node and the remaining nodes are fictitious load points. The fictitious source node and fictitious load node are the source and the destination of fictitious power flow, respectively. The amount of the fictitious flow into a load node $d_{i,t}^{\text{fic}}$ is set as 1 at all nodes. The second condition is satisfied in constraints (17)–(19) that enforce each load node to receive one unit of the fictitious flow from the fictitious source node at each PI. Constraints (17) and (18) ensure the fictitious flow balance for the fictitious load and source nodes, respectively. Constraint (19) enforces the fictitious flow to be zero in open branches. The large enough positive number M relaxes this constraint when some branches are open (see [34] for additional details on the fictitious network and radiality conditions)

$$\sum_{(i,j)\in\mathbf{L}} \alpha_{ij,t} = N_{\mathbf{B}} - N_t^{\text{island}} \quad \forall t \in \mathbf{T} \tag{16}$$

$$\sum_{(j,i)\in\mathbf{L}} fl_{ji,t} - \sum_{(i,j)\in\mathbf{L}} fl_{ij,t} = d_{i,t}^{\text{fic}} \quad \forall i \in \mathbf{B}\backslash\mathbf{B}_t^{\text{source}} \quad \forall t \in \mathbf{T} \tag{17}$$

$$\sum_{(i,j)\in\mathbf{L}} fl_{ij,t} - \sum_{(j,i)\in\mathbf{L}} fl_{ji,t} = fg_{i,t} \quad \forall i \in \mathbf{B}_t^{\text{source}} \quad \forall t \in \mathbf{T} \tag{18}$$

$$-\alpha_{ij,t}\cdot M \le fl_{ij,t} \le \alpha_{ij,t}\cdot M \quad \forall (i,j)\in\mathbf{L} \quad \forall t\in\mathbf{T}. \tag{19}$$

E. Branch Status Constraints

According to (20), the damaged branch must be open if it has not yet been repaired at time t. Constraint (21) states that the undamaged branches without RCS remain in their initial status over all time periods

$$\alpha_{ij,t} \le \beta_{ij,t} \quad \forall (i,j)\in\mathbf{L} \quad \forall t\in\mathbf{T} \tag{20}$$

$$\alpha_{ij,t} = \alpha_{ij}^0 \quad \forall (i,j)\in\mathbf{L}\left\backslash\left\{\mathbf{L}_t^{\text{damaged}}, \mathbf{L}^{\text{switch}}\right\}\right. \quad \forall t\in\mathbf{T}. \tag{21}$$

F. MPS Output Power Constraints

Constraints (22) and (23) indicate that the real or reactive power injection or extraction at a candidate node for MPS siting is equal to the sum of the real or reactive power output of the MPSs. The non-MPS nodes are attributed zero real and reactive power from MPSs as expressed in (24)

$$p_{i,t}^{\text{mps}} = \sum_{m\in\mathbf{M}_i\cap\{\mathbf{S},\mathbf{V}\}} \mu_{m,i,t}\cdot p_{m,t}^{\text{dch}} - \sum_{m\in\mathbf{M}_i\cap\{\mathbf{S},\mathbf{V}\}} \mu_{m,i,t}\cdot p_{m,t}^{\text{ch}} + \sum_{m\in\mathbf{M}_i\cap\mathbf{G}} \mu_{m,i,t}\cdot p_{m,t} \quad \forall i \in \bigcup_{m\in\mathbf{M}} \mathbf{B}_m \quad \forall t\in\mathbf{T} \tag{22}$$

$$q_{i,t}^{\text{mps}} = \sum_{m\in\mathbf{M}_i} \mu_{m,i,t}\cdot q_{m,t} \quad \forall i \in \bigcup_{m\in\mathbf{M}} \mathbf{B}_m \quad \forall t\in\mathbf{T} \tag{23}$$

$$p_{i,t}^{\text{mps}} = q_{i,t}^{\text{mps}} = 0 \quad \forall i \in \mathbf{B}\backslash\bigcup_{m\in\mathbf{M}} \mathbf{B}_m \quad \forall t\in\mathbf{T}. \tag{24}$$

G. Power Balance Constraints

Constraints (25) and (26) describe the real and reactive power balance conditions at all nodes, respectively. The range of the demanded load to be supplied is bounded in constraint (27). Constraint (28) enforces the recovery rate of the supplied loads not to decrease. The power factor of the demand is assumed to be fixed in (29). The real and reactive power flows in the online branches are, respectively, limited by their real and reactive power capacities in (30) and (31). Constraints (30) and (31) also enforce the real and reactive power flow in open branches to be zero

$$\sum_{(j,i)\in\mathbf{L}} pf_{ji,t} - \sum_{(i,j)\in\mathbf{L}} pf_{ij,t} = pd_{i,t} - pg_{i,t} - p_{i,t}^{\text{mps}} \quad \forall i\in\mathbf{B} \quad \forall t\in\mathbf{T} \tag{25}$$

$$\sum_{(j,i)\in\mathbf{L}} qf_{ji,t} - \sum_{(i,j)\in\mathbf{L}} qf_{ij,t} = qd_{i,t} - qg_{i,t} - q_{i,t}^{\text{mps}} \quad \forall i\in\mathbf{B} \quad \forall t\in\mathbf{T} \tag{26}$$

$$0 \le pd_{i,t} \le P_{i,t}^{\text{demand}} \quad \forall i\in\mathbf{B} \quad \forall t\in\mathbf{T} \tag{27}$$

$$pd_{i,t-1}/P_{i,t-1}^{\text{demand}} \le pd_{i,t}/P_{i,t}^{\text{demand}} \quad \forall i\in\mathbf{B} \quad \forall t\ge 1 \tag{28}$$

$$qd_{i,t} = \left(Q_{i,t}^{\text{demand}}/P_{i,t}^{\text{demand}}\right)\cdot pd_{i,t} \quad \forall i\in\mathbf{B} \quad \forall t\in\mathbf{T} \tag{29}$$

$$-\alpha_{ij,t}\cdot\overline{P}_{ij} \le pf_{ij,t} \le \alpha_{ij,t}\cdot\overline{P}_{ij} \quad \forall (i,j)\in\mathbf{L} \quad \forall t\in\mathbf{T} \tag{30}$$

$$-\alpha_{ij,t}\cdot\overline{Q}_{ij} \le qf_{ij,t} \le \alpha_{ij,t}\cdot\overline{Q}_{ij} \quad \forall (i,j)\in\mathbf{L} \quad \forall t\in\mathbf{T}. \tag{31}$$

H. Power Flow Constraints

Constraints (32) and (33) represent the power flow equation in which the *M* value is a relaxation parameter [35]. Constraint (34) states the boundary for the voltage magnitudes

$$V\text{sqr}_{i,t} - V\text{sqr}_{j,t} \le (1-\alpha_{ij,t})\cdot M + 2\cdot(r_{ij}\cdot pf_{ij,t} + x_{ij}\cdot qf_{ij,t}) \quad \forall (i,j)\in\mathbf{L} \quad \forall t\in\mathbf{T} \tag{32}$$

$$V\text{sqr}_{i,t} - V\text{sqr}_{j,t} \ge (\alpha_{ij,t}-1)\cdot M + 2\cdot(r_{ij}\cdot pf_{ij,t} + x_{ij}\cdot qf_{ij,t}) \quad \forall (i,j)\in\mathbf{L} \quad \forall t\in\mathbf{T} \tag{33}$$

$$\underline{\text{Vsqr}}_i \le V\text{sqr}_{i,t} \le \overline{\text{Vsqr}}_i \quad \forall i\in\mathbf{B} \quad \forall t\in\mathbf{T}. \tag{34}$$

Note that constraints (22) and (23) include nonlinear terms making the optimization problem an MINLP) model. We propose a linearization technique, which is as

follows [36]:

$$0 \le P^{\text{dch}}_{m,i,t} \le \mu_{m,i,t} \cdot \overline{P}^{\text{dch}}_{m} \tag{35}$$

$$p^{\text{dch}}_{m,t} + (\mu_{m,i,t} - 1) \cdot \overline{P}^{\text{dch}}_{m} \le P^{\text{dch}}_{m,i,t} \le p^{\text{dch}}_{m,t} \tag{36}$$

where if $\mu_{m,i,t} = 1$, then we have $P^{\text{dch}}_{m,i,t} = p^{\text{dch}}_{m,t}$; if $\mu_{m,i,t} = 0$, then $P^{\text{dch}}_{m,i,t} = 0$. By doing so, the MINLP formulation is linearized into an MILP problem and, therefore, the computation complexity is significantly reduced.

IV. Numerical Results and Discussions

A. Test Case I: The Benchmark System

1) Test System Description: In order to verify the effectiveness of the proposed scheme for DS seismic resilience, the IEEE 33-node test system is employed as the testbed. The total time period is considered $T = 24$, where each time period accounts for $\Delta t = 0.5$ h. All the MPSs are located at the substation node at $t = 1$ and the initial SOC of EV and MESS are considered fully charged. To investigate the impact of MPSs sizing on the load restoration performance during emergencies, we here study three different scenarios: *Scenario 1*, where the three MPSs have their original sizing; *Scenario 2*, where the size of all three MPSs has been increased to 1.5 times of their original values; and *Scenario 3*, where there are four MPSs: two EVs, one MESS, and one MEG. Note that the term "size" here refers to both "the rated power" and "capacity" of any type of MPS. In all cases, the same type of MPS is taken with the same configuration (rated power, capacity, efficiency, travelling cost, etc.). All simulations have been conducted on a PC with an Intel Xeon E5-2620 v2 processor and 16 GB of memory using CPLEX 12.5.1.

2) Seismic Hazard Characterization: The earthquake energy propagation and attenuation is highly dependent on the pattern the seismic waves pass through, e.g., soil and sediments. We assumed that the soil type at the location of the test case is mostly of rock. According to Nazemi and Dehghanian [37], one may consider the rock-type equivalent to shear wave velocities higher than or equal to 375 m/s. Inspired by Nazemi *et al.* [38], the specific AR used in this study is described as follow:

$$\ln(G_a) = 4.15 + 0.623\left(\frac{M_W + 0.38}{1.06}\right) + 0.96\ln(R) \tag{37}$$

where G_a is PGA, M_W is the earthquake intensity with moment magnitude, and R is the epicenter distance between the source of the earthquake and the studied system. In the context of seismic analysis and design of structures, various earthquake data may be required depending upon the nature of analysis being carried out. The acceleration and displacement response spectrum of an earthquake are the most favored seismic input for earthquake engineers. Fig. 3(a) illustrates the simulated earthquake accelerogram used in this study. The duration of earthquake is considered 1 min, Fig. 3(b) represents the displacement response spectra of a single degree of freedom (SDOF) to a particular ground motion used in our analysis. Fig. 3(c) illustrates pseudoacceleration response spectrum of a given input seismic earthquake for 2% damping. Fig. 3(d) represents the logarithmic acceleration response spectra with 2% damping.

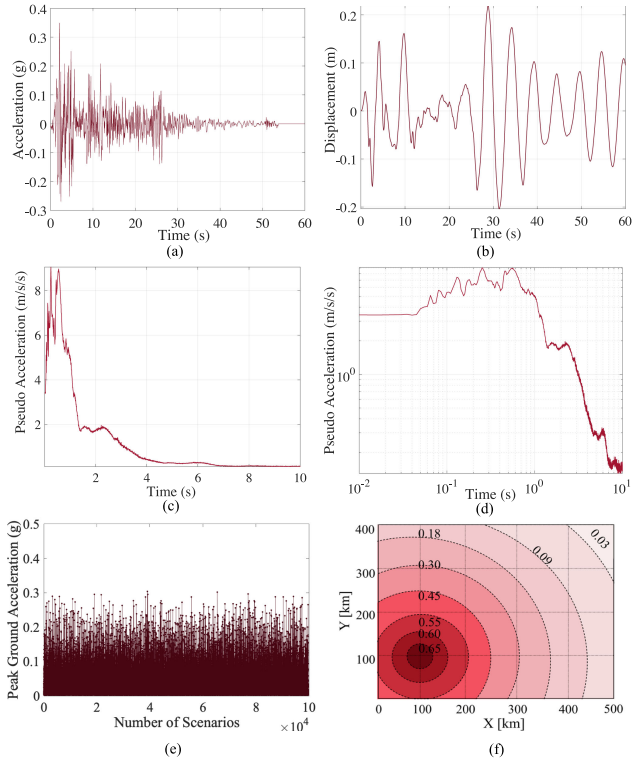

Fig. 3. Seismic statistics assumptions. (a) Simulated earthquake accelerogram. (b) Response of SDOF system with 2% damping and natural period of 5 s. (c) Pseudoacceleration response spectrum of the studied earthquake for 2% damping. (d) Logarithmic pseudoacceleration response spectrum of the studied earthquake for 2% damping. (e) Evaluated PGA at the location of power distribution branches considering all scenarios generated by MCS. (f) PGA logarithmic attenuation for a specific earthquake realization with an epicenter at (100, 100) km. PGA values shown above each contour are in (g).

Fig. 3(e) reflects the evaluated PGA at the location of power distribution branches considering all acceptable earthquake scenarios generated by MCS. Fig. 3(f) shows PGA attenuation for a particular earthquake realization. For the earthquakes' location, we use randomly generated uniformly distributed locations in 500×500 km^2, as shown in Fig. 3, which also shows the PGA attenuation for a particular earthquake realization.

3) MPSs Routing and Scheduling: The set of damaged branches in the network L^{damaged} in the face of simulated earthquake scenarios are illustrated in Fig. 4 at time slot $t = 1 \sim 2$. The allocation of eight RCS is also demonstrated in Fig. 4. We generated 100 000 earthquake scenarios via the MCS, where it was identified that 9 branches out of the 37 branches in the network have a remarkable fragility comparatively [39], [40]. The repair schedule for damaged branches is assumed as follows: branch 19–20 at $t = 3$, branch 8–9 at $t = 6$, branch 9–10 at $t = 7$, branch 12–13 at $t = 9$, branch 16–17 at $t = 13$, branch 30–31 at $t = 16$, branch 27–28 at $t = 20$, branch 24–25 at $t = 22$, and branch 23–24 at $t = 24$ will be repaired. The restoration process for scenario 1 is demonstrated in Fig. 4, where only some restoration time periods are presented. The location of MPSs at each time period during the restoration phase for all scenarios is illustrated in Fig. 5 in which the symbol "$\rightarrow$" denotes that the MPS is travelling between different nodes. The power profile

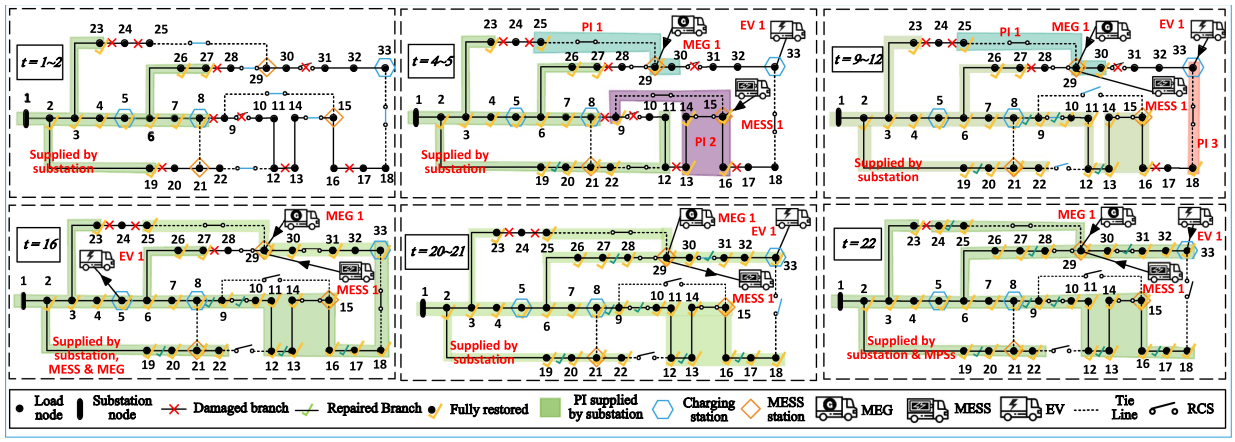

Fig. 4. Restoration process coordinated with MPSs dispatch and DS dynamic reconfiguration.

Scenario 1		Time Period								
		1	2~3	4~6	7	8~12	13~14	15~16	17~18	19~24
MPS	EV 1	node 1	→	node 33			→	node 5	→	node 33
	MESS 1	node 1	→	node 15	→	node 29				
	MEG 1	node 1	→	node 29						

Scenario 2		Time Period										
		1	2~3	4~7	8	9	10	11~12	13~14	15	16	17~18	19~24
MPS	EV 1	node 1	→	node 33					→	node 5	→		node 33
	MESS 1	node 1	→	node 15	→	node 29	→	node 15	→	node 29			
	MEG 1	node 1	→	node 29									

Scenario 3		Time Period												
		1	2~3	4~5	6	7	8	9~10	11~12	13~14	15	16	17	18~19	20~21	22~24
MPS	EV 1	node 1	→	node 33					→	node 5	→		node 33			
	MESS 1	node 1	→	node 15	→	node 29										
	MEG 1	node 1	→	node 29												
	EV 2	node 1	→	node 33	→		node 8	→	node 33		→		node 5	→		node 33

Fig. 5. Location of MPSs at each time period during the restoration process for all scenarios (TC 1).

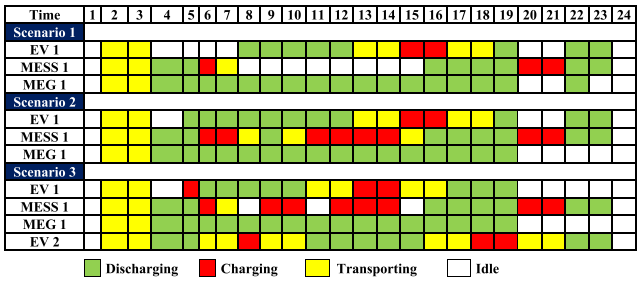

Fig. 6. MPSs' power profile in each time period in different scenarios (TC 1).

of the MPSs at each time period during the restoration process for all three scenarios is illustrated in Fig. 6. In the following, detailed discussions on the system restoration in *scenario 1* are provided.

At $t = 1\sim2$, tie lines 9–15, 12–22, 18–33, and 25–29, which are normally open (i.e., offline), should be closed (i.e., online) in order to change the DS topology such that several PIs can be linked to facilitate the MPSs contribution in recovery of load outages in the subsequent time periods. Note that branches 14–15 and 28–29 are already online during the normal operating conditions, whereas branches 9–10 and 30–31 are offline due to postquake damages. Besides, all MPSs should be departed from the substation node at time $t = 1$. At $t = 4\sim5$, branch 19–20 has been repaired by repair crews; MEG 1 and MESS 1 are connected to node 29 and node 15, respectively, to form PI 1 and PI 2. While EV 1 reaches the node 33, it should not be discharged since the energy is reserved for the subsequent recovery time periods. At $t = 6$, branch 8–9 is repaired and closed. Consequently, MESS 1 and PI 2 can access to the main grid, and MESS 1 is charging to reserve more energy for the subsequent recovery time periods. At $t = 7$, since branch 9–10 is repaired and connected back, branch 12–22 is open to ensure the DS radial topology. Meanwhile, MESS 1 departs from node 15 since the load points in PI 2 can be supplied by the main grid and no longer need the power supply from MESS 1. At $t = 8$, EV 1 starts supplying power in PI 3 and MESS 1 arrives at node 29. According to Figs. 5 and 6, MESS 1 will stay at node 29 until the end of the restoration and should not be discharged at $t = 8\sim15$ since the energy is reserved for the subsequent recovery time periods. At $t = 9$, branch 9–15 is open to ensure the DS radial topology since branch 12–13 is repaired and connected back. At $t = 13$, branch 16–17 is repaired; hence, nodes 17, 18, and 33 are reconnected to the substation node and PI 3 is merged with the main grid. Meanwhile, EV 1 starts traveling to node 5 to connect to the main grid and gets charged at $t = 15\sim16$ since its SOC is reaching the minimum threshold. At $t = 16$, branch 30–31 is repaired and MESS 1 starts discharging to supply nodes 31–33. At $t = 17$, EV 1 departs node 5 since it gets enough energy. At $t = 19$, EV 1 arrives at node 33 and continues supplying the neighbor load points as they have not been yet fully restored—due to the distribution lines capacity limits. At $t = 20$, branch 27–28 is repaired and re-energized; therefore, branch 18–33 is open to ensure the DS radial topology. At this time, all the load points across the studied DS, except node 24, are connected back to the main grid. Since the neighbor nodes can be directly supplied by the main grid, EV 1 and MEG 1 stop supplying power at $t = 20\sim21$ and reserve the energy for subsequent time periods. Meanwhile, MESS 1 is charging itself for the same purpose. At $t = 22$, branch 24–25 is repaired, the DS is fully restored by the main grid substation and all the grid-support MPS resources even though branch 23–24 is not yet repaired.

In order to highlight the accuracy of the results, four restoration strategies are studied: *Case 1*, the benchmark (with neither

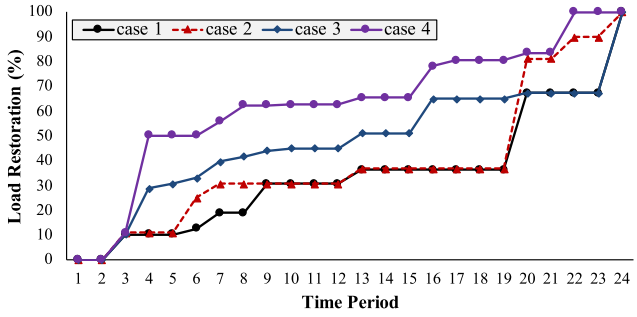

Fig. 7. Load restoration in each restoration time period in different studied cases (TC 1).

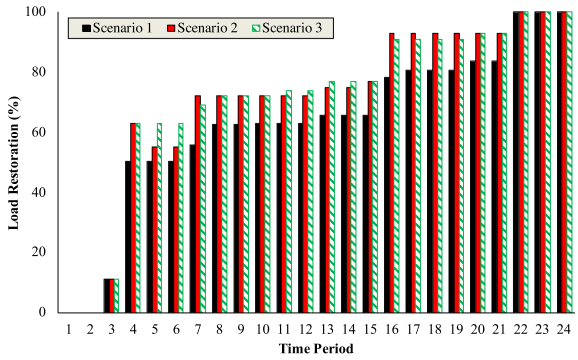

Fig. 8. Load restoration comparison in different scenarios (TC 1).

DS reconfiguration nor MPS supply); *Case 2*, considering only DS reconfiguration without MPS supply; *Case 3*, considering only MPS supply without any DS reconfiguration; and *Case 4*, the proposed method (using both DS reconfiguration and MPS supply). The load restoration results are compared in Fig. 7. One can see that the proposed approach reveals the highest load restoration through the entire restoration process, whereas the benchmark has resulted in the lowest. Furthermore, Case 3 with only MPS supply has higher restoration percentage at early time periods ($t = 4\sim19$) since the distribution lines are damaged and the MPSs have supplied the outage areas and effectively restored the loads that cannot be otherwise restored by the main grid. However, at the later time periods ($t = 20\sim23$), *Case 2* has shown higher load restoration percentages than that in *Case 3*. In *Case 3*, MPS can supply some outage loads; however, due to the damaged lines with no DS reconfiguration action applied, the available lines with RCS are not fully utilized and the power cannot be delivered to additional outage loads. In *Case 2*, even though the distribution grid has no extra electricity source to supply the outage area, the DS reconfiguration fully utilized the available lines with RCS and let the power from the main grid be delivered to the outage areas. Thus, as Fig. 7 shows, the proposed method (using both DS reconfiguration and MPS supply) is the most effective approach during the restoration process. In summary, the proposed model for utilizing the MPSs conjointly with harnessing the built-in flexibility of the DS topology (through DS dynamic reconfiguration) has resulted in 100% load outage recovery at $t = 22$, as shown in Fig. 7. Fig. 8 represents the difference in load restoration percentage at each time period in three different scenarios. One can see that the scenarios 2 and 3 in which either the size of MPSs is bigger or the number of MPSs is higher, the load restoration percentage is higher in the most time periods. This further highlights the role of the MPSs in DS restoration if well planned, scheduled, and coordinated with other flexible resources.

B. Test Case 2: Higher Earthquake Intensity

To highlight the accuracy of the results, we assumed another test case considering a higher earthquake intensity that leads to more distribution branches being unavailable following the event. In this test case, we identified 12 damaged branches that

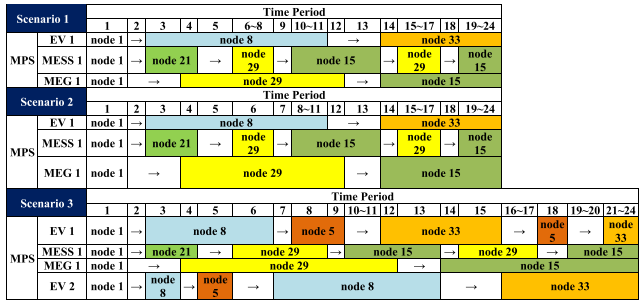

Fig. 9. Location of MPSs at each restoration time period in different scenarios (TC 2)

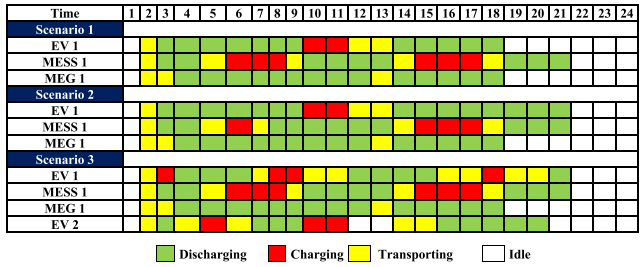

Fig. 10. MPSs power profile in each time period in different scenarios (TC 2).

would be out of service with the following repair schedules: branch 1–2 at $t = 3$, branch 19–20 at $t = 5$, branch 23–24 at $t = 7$, branch 5–6 at $t = 8$, branch 7–8 at $t = 10$, branch 26–27 at $t = 13$, branch 25–29 at $t = 16$, branch 9–15 at $t = 17$, branch 32–33 at $t = 19$, branch 17–18 at $t = 22$, branch 12–13 at $t = 23$, and branch 11–12 at $t = 24$ will be repaired. Similar to the test case 1 (benchmark), Figs. 9 and 10 represent, respectively, the location of MPSs and the MPSs power profile at each restoration time period in all three assumed scenarios. Fig. 11 illustrates the load restoration percentage comparison in three different scenarios. One can see from the results that the more the number of MPSs, the higher the load restoration percentage during majority of the time periods. The numerical results verified that the proposed model can not only effectively reduce the amount of load outages, but also ensures a swift response and recovery, thereby realizing an enhanced operational resilience to HILP earthquakes.

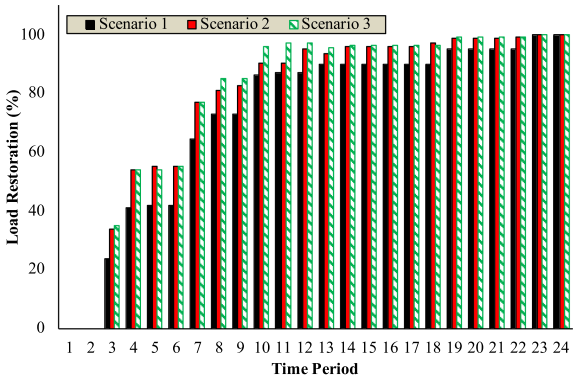

Fig. 11. Load restoration comparison in different scenarios (TC 2).

V. Discussions and Practical Considerations

In the following, we discuss several practical considerations that should be accounted for if aiming to implement the proposed approach in practice under real-world scenarios.

1) Following a seismic hazard, both generation and load profiles are constantly changing. The conventional approaches for frequency control and protection have only one set point for all scenarios. Offline power generators' loading optimization is a common practice for electric power utilities in order to prevent dangerous imbalance between load and generation and strong frequency deviations during power system restorations. A major deficiency in conventional approaches for frequency control during power system restoration is that local protection devices do not have a system view, and therefore, they are not able to take optimized and coordinated actions. Nonetheless, we assumed that the power system is equipped with a wide area measurement system frequency control mechanism that can customize frequency control algorithms dynamically in response to any system condition. Besides, in this article, we assumed that prior to synchronizing multiple microgrid, the transmission system operators adjust the frequency of the smaller subsystem (microgrid) to match the frequency of the larger area. In addition, the voltages in two areas or subsystems are as close as possible prior to synchronization. Upon synchronization, the regulation requirement for frequency control must be recalculated and reassigned. After synchronization, the transmission operators calculate reserve requirements for the combined system and adjust unit dispatch accordingly. Area (or subsystem) frequency is maintained above 59.75 Hz and below 61.0 Hz. Achieving and maintaining these frequency levels require close coordination between generation, transmission, and distribution operators.
2) The distribution branches that are considered in the article include poles, wires, in-line equipment, utility-owned equipment, and overhead conductors. We assume that the type of conductors is most likely of one of these categories: all aluminum alloy conductor, aluminum conductor steel reinforced, or all aluminum conductor. Since power distribution branches do not have the same response to earthquake shocks, five damage states—none, slight, moderate, extensive, and complete damage—which, respectively, denote 0%, 4%, 12%, 50%, and 80% of all distribution lines [37], [38], are introduced in this article to assess the postquake availability of power distribution branches all across the network.
3) A severe seismic hazard might also affect other critical facilities, such as transportation and communication networks. In case of severe earthquake hazards, the potentials of MPSs cannot be fully harnessed due to partial or full postquake unavailability of the transportation network elements, such as bridges, highways, streets, etc. Future research should integrate both power network and transportation systems to account for the interdependencies and accessibility limitations due to damaged roads, highways, and bridges. Such realistic constraints should be further analyzed that may prevent otherwise the practical implementation of the proposed solutions during emergencies.

VI. Conclusion

This article proposes a co-optimization approach to improve the DS operational resilience in dealing with the aftermath of HILP seismic hazards. Seismic hazard characterization is accomplished by a suite of simulated earthquake scenarios via an MCS engine to evaluate the fragility (vulnerability) of the distribution branches in the face of seismic forces. An MINLP optimization model is suggested, linearized, and reformulated to an MILP model in order to achieve an effective restoration strategy that unlocks the full potential of MPSs (effective routing and scheduling) and the dynamic DS network reconfiguration (effective utilization of the grid built-in flexibility using the existing infrastructure), all in coordination with the repair crew schedules. Numerical results demonstrated that the proposed approach could effectively facilitate the DS restoration through a swift response and recovery, resulting in a significant reduction in the outage extent and duration, thereby realizing an enhanced operational resilience to HILP earthquakes.

References

[1] B. Zhang, P. Dehghanian, and M. Kezunovic, "Optimal allocation of PV generation and battery storage for enhanced resilience," *IEEE Trans. Smart Grid*, vol. 10, no. 1, pp. 535–545, Jan. 2019.
[2] P. Dehghanian, S. Aslan, and P. Dehghanian, "Maintaining electric system safety through an enhanced network resilience," *IEEE Trans. Ind. Appl.*, vol. 54, no. 5, pp. 4927–4937, Sep./Oct. 2018.
[3] S. Wang, L. Li, and P. Dehghanian, "Power grid online surveillance through PMU-embedded convolutional neural networks," in *Proc. IEEE Ind. Appl. Soc. Annu. Meet.*, Sep. 2019, pp. 1–8.
[4] S. Wang, P. Dehghanian, L. Li, and B. Wang, "A machine learning approach to detection of geomagnetically induced currents in power grids," in *Proc. IEEE Ind. Appl. Soc. Annu. Meet.*, Sep. 2019, pp. 1–7.
[5] Major California Earthquakes, 1989. [Online] Available: https://cnico.com/pgs/earthquake/earth3.aspx
[6] R. J. Campbell, "Weather-related power outages and electric system resiliency," Congressional Research Service, Library of Congress, Washington, DC, USA, 2012.
[7] Y. Kitagawa and H. Hiraishi, "Overview of the 1995 Hyogo-Ken Nanbu earthquake and proposals for earthquake mitigation measures," *J. Jpn. Assoc. Earthq. Eng.*, vol. 4, no. 3, pp. 1–29, 2004.
[8] M. Ghafory-Ashtiany and M. Hosseini, "Post-bam earthquake: Recovery and reconstruction," *Natural Hazards*, vol. 44, no. 2, pp. 229–241, 2008.

[9] J. Eidinger, "Wenchuan earthquake impact to power systems," in *Proc. TCLEE: Lifeline Earthq. Eng. Multihazard Environ.*, 2009, pp. 1–12.
[10] Y. Kuwata and Y. Ohnishi, "Emergency-response capacity of lifelines after wide-area earthquake disasters," in *Proc. Int. Symp. Eng. Lessons Learned Great East Jpn. Earthq.*, 2011, pp. 1475–1486.
[11] M. Zare, F. Kamranzad, I. Parcharidis, and V. Tsironi, "Preliminary report of Mw7.3 Sarpol-e Zahab, Iran earthquake on November 12, 2017," Int. Inst. Earthq. Eng. Seismology, Tehran, Iran, Tech. Rep., 2017.
[12] P. Dehghanian, B. Zhang, T. Dokic, and M. Kezunovic, "Predictive risk analytics for weather-resilient operation of electric power systems," *IEEE Trans. Sustain. Energy*, vol. 10, no. 1, pp. 3–15, Jan. 2019.
[13] M. Nazemi, P. Dehghanian, and M. Lejeune, "A mixed-integer distributionally robust chance-constrained model for optimal topology control in power grids with uncertain renewables," in *Proc. IEEE Milan PowerTech*, 2019, pp. 1–6.
[14] J. Su, P. Dehghanian, M. Nazemi, and B. Wang, "Distributed wind power resources for enhanced power grid resilience," in *Proc. 51th North Amer. Power Symp.*, Wichita, KS, USA, Oct. 2019, pp. 1–6.
[15] K. P. Schneider, F. K. Tuffner, M. A. Elizondo, C.-C. Liu, Y. Xu, and D. Ton, "Evaluating the feasibility to use microgrids as a resiliency resource," *IEEE Trans. Smart Grid*, vol. 8, no. 2, pp. 687–696, Mar. 2017.
[16] J. Lai, X. Lu, F. Wang, P. Dehghanian, and R. Tang, "Broadcast gossip algorithms for distributed peer-to-peer control in ac microgrids," *IEEE Trans. Ind. Appl.*, vol. 55, no. 3, pp. 2241–2251, May/Jun. 2019.
[17] P. M. de Quevedo, J. Contreras, A. Mazza, G. Chicco, and R. Porumb, "Reliability assessment of microgrids with local and mobile generation, time-dependent profiles, and intraday reconfiguration," *IEEE Trans. Ind. Appl.*, vol. 54, no. 1, pp. 61–72, Jan./Feb. 2018.
[18] Y. Xu, C.-C. Liu, K. P. Schneider, F. K. Tuffner, and D. T. Ton, "Microgrids for service restoration to critical load in a resilient distribution system," *IEEE Trans. Smart Grid*, vol. 9, no. 1, pp. 426–437, Jan. 2018.
[19] J. Kim and Y. Dvorkin, "Enhancing distribution system resilience with mobile energy storage and microgrids," *IEEE Trans. Smart Grid*, vol. 10, no. 5, pp. 4996–5006, Sep. 2019.
[20] S. Lei, C. Chen, Y. Li, and Y. Hou, "Resilient disaster recovery logistics of distribution systems: Co-optimize service restoration with repair crew and mobile power source dispatch," *IEEE Trans. Smart Grid*, vol. 10, no. 6, pp. 6187–6202, Nov. 2019.
[21] B. Wang, J. A. Camacho, G. M. Pulliam, A. H. Etemadi, and P. Dehghanian, "New reward and penalty scheme for electric distribution utilities employing load-based reliability indices," *IET Gener., Transmiss. Distrib.*, vol. 12, no. 15, pp. 3647–3654, 2018.
[22] Y. Ma, T. Houghton, A. Cruden, and D. Infield, "Modeling the benefits of vehicle-to-grid technology to a power system," *IEEE Trans. Power Syst.*, vol. 27, no. 2, pp. 1012–1020, May 2012.
[23] S. Lei, C. Chen, H. Zhou, and Y. Hou, "Routing and scheduling of mobile power sources for distribution system resilience enhancement," *IEEE Trans. Smart Grid*, vol. 10, no. 5, pp. 5650–5662, Sep. 2019.
[24] H. Shin and R. Baldick, "Plug-in electric vehicle to home (V2H) operation under a grid outage," *IEEE Trans. Smart Grid*, vol. 8, no. 4, pp. 2032–2041, Jul. 2017.
[25] S. Lei, J. Wang, C. Chen, and Y. Hou, "Mobile emergency generator pre-positioning and real-time allocation for resilient response to natural disasters," *IEEE Trans. Smart Grid*, vol. 9, no. 3, pp. 2030–2041, May 2018.
[26] J. A. Taylor and F. S. Hover, "Convex models of distribution system reconfiguration," *IEEE Trans. Power Syst.*, vol. 27, no. 3, pp. 1407–1413, Aug. 2012.
[27] T. E. McDermott, I. Drezga, and R. P. Broadwater, "A heuristic nonlinear constructive method for distribution system reconfiguration," *IEEE Trans. Power Syst.*, vol. 14, no. 2, pp. 478–483, May 1999.
[28] Y.-K. Wu, C.-Y. Lee, L.-C. Liu, and S.-H. Tsai, "Study of reconfiguration for the distribution system with distributed generators," *IEEE Trans. Power Del.*, vol. 25, no. 3, pp. 1678–1685, Jul. 2010.
[29] R. S. Rao, K. Ravindra, K. Satish, and S. Narasimham, "Power loss minimization in distribution system using network reconfiguration in the presence of distributed generation," *IEEE Trans. Power Syst.*, vol. 28, no. 1, pp. 317–325, Feb. 2013.
[30] O. W. Nuttli, "Seismic wave attenuation and magnitude relations for eastern north america," *J. Geophys. Res.*, vol. 78, no. 5, pp. 876–885, 1973.
[31] C. A. Kircher, R. V. Whitman, and W. T. Holmes, "Hazus earthquake loss estimation methods," *Natural Hazards Rev.*, vol. 7, no. 2, pp. 45–59, 2006.
[32] "Multi-hazard loss estimation methodology, earthquake model," Federal Emergency Management Agency, Washington, DC, USA, HAZUS-MH User's Manual, 2003.
[33] S. Iwai, T. Kono, M. Hashiwaki, and Y. Kawagoe, "Use of mobile engine generators as source of back-up power," in *Proc. IEEE 31st Int. Telecommun. Energy Conf.*, 2009, pp. 1–6.
[34] M. Lavorato, J. F. Franco, M. J. Rider, and R. Romero, "Imposing radiality constraints in distribution system optimization problems," *IEEE Trans. Power Syst.*, vol. 27, no. 1, pp. 172–180, Feb. 2012.
[35] M. E. Baran and F. F. Wu, "Network reconfiguration in distribution systems for loss reduction and load balancing," *IEEE Trans. Power Del.*, vol. 4, no. 2, pp. 1401–1407, Apr. 1989.
[36] W. Wei, F. Liu, S. Mei, and Y. Hou, "Robust energy and reserve dispatch under variable renewable generation," *IEEE Trans. Smart Grid*, vol. 6, no. 1, pp. 369–380, Jan. 2015.
[37] M. Nazemi and P. Dehghanian, "Seismic-resilient bulk power grids: Hazard characterization, modeling, and mitigation," *IEEE Trans. Eng. Manage.*, to be published, doi: 10.1109/TEM.2019.2950669.
[38] M. Nazemi, M. Moeini-Aghtaie, M. Fotuhi-Firuzabad, and P. Dehghanian, "Energy storage planning for enhanced resilience of power distribution networks against earthquakes," *IEEE Trans. Sustain. Energy*, to be published, doi: 10.1109/TSTE.2019.2907613.
[39] Z. Yang, M. Nazemi, P. Dehghanian, and M. Barati, "Toward resilient solar-integrated distribution grids: Harnessing the mobility of power sources," *Proc. IEEE Power Energy Soc. Transmiss. Distrib. Conf. Expo.*, Chicago, IL, USA, Apr. 2020, pp. 1–5.
[40] Z. Yang, P. Dehghanian, and M. Nazemi, "Enhancing seismic resilience of electric power distribution systems with mobile power sources," *IEEE Ind. Appl. Soc. Annu. Meet.*, Baltimore, MD, USA, pp. 1–7, Sep./Oct. 2019.

Zijiang Yang (Student Member, IEEE) received the B.Sc. degree in electrical engineering from the North China Electric Power University, Beijing, China and the Illinois Institute of Technology, Chicago, IL, USA, in 2017, and the M.Sc. degree in electrical engineering from The George Washington University, Washington, DC, USA, in 2019.

He is currently an Engineer with the China Energy Engineering Group, Guangdong Electric Power Design Institute Company, Ltd., Guangdong, China. His research interests include power system reliability and resiliency, energy optimizations, and smart electricity grid applications.

Payman Dehghanian (Member, IEEE) received the B.Sc. degree in electrical engineering from the University of Tehran, Tehran, Iran, in 2009, the M.Sc. degree in electrical engineering from the Sharif University of Technology, Tehran, Iran, in 2011, and the Ph.D. degree in electrical engineering from Texas A&M University, College Station, TX, USA, in 2017.

He is an currently an Assistant Professor with the Department of Electrical and Computer Engineering, The George Washington University, Washington, DC, USA. His research interests include power system protection and control, power system reliability and resiliency, asset management, and smart electricity grid applications.

Dr. Dehghanian was the recipient of the 2013 IEEE Iran Section Best M.Sc. Thesis Award in electrical engineering, the 2014 and 2015 IEEE Region 5 Outstanding Professional Achievement Awards, and the 2015 IEEE-HKN Outstanding Young Professional Award.

Mostafa Nazemi (Student Member, IEEE) received the B.Sc. degree in electrical engineering from the K. N. Toosi University of Technology, Tehran, Iran, in 2015, and the M.Sc. degree in energy systems engineering from the Sharif University of Technology, Tehran, Iran, in 2017. He is currently working toward the Ph.D. degree in electrical engineering with the Department of Electrical and Computer Engineering, The George Washington University, Washington, DC, USA.

His research interests include power system resilience, power system planning and operation, energy optimizations, and smart electricity grid applications.

Mr. Nazemi was the recipient of the 2018 Certificate of Excellence in Reviewing by the Editorial Board Committee of the *Journal of Modern Power and Clean Energy* for his contributions to the journal.